Benha Journal of Applied Sciences (BJAS) **print: ISSN 2356–9751**
Vol. (6) Issue (6) Part (1) (2021), (107-118) **online: ISSN 2356–976x**
http://bjas.journals.ekb.eg

Removal of Acid Blue 342 from Aqueous Solution by Fe_2O_3/Fe_3O_4 Magnetic Nanocomposite

H.H.El-Feky, G.O.El-Sayed and R.R.Shalabi
Chemistry, Dept., Faculty of Science, Benha Univ., Benha, Egypt
E-mail: hesham.elfeky@fsc.bu.edu.eg

Abstract

The synthesis, characterization and capacity studies of fabricated magnetic Fe_2O_3/Fe_3O_4 nanocomposites capable of adsorbing with Acid Blue 342 dye (AB) were reported. The product was characterized by FT-IR, XRD, SEM and TEM techniques. The crystallite size calculated using the Scherrer formula for the fabricated nanocomposite was about 22.38 nm. The results of SEM analysis show rough surfaces and many visible fluffy mesoporous. The adsorption properties of the Fe_2O_3/Fe_3O_4 nanocomposites for the removal of Acid Blue 342 dye (AB) were examined. By using a batch method, various parameters affecting the adsorption properties were studied. The results revealed that Fe_2O_3/Fe_3O_4 nanostructure gave high adsorption capacity equal 39.45 mg/g. The equilibrium isotherm, kinetics parameters of the adsorption process were also calculated. The study indicated that the pseudo second-order adsorption mechanism is predominate and that the overall rate of the AB dye adsorption process was controlled by the chemisorption process.

Keywords: magnetic nanoparticles, adsorption isotherm, kinetics, Acid Blue 342.

1. Introduction

The flow of a large number of contaminants in wastewater, including organic and inorganic pollutants such as pesticides, dyes, heavy metals, and other toxins, is mostly due to rising population and rapid industrialization [1-3]. Direct discharge of partly or untreated wastewater into surface water bodies poses a significant challenge for humans, providing considerable environmental concerns that affect the food chain and, as a result, human health via bio-accumulation and bio-magnification [4-6]. To prevent or limit the harmful impacts of water pollutants, many tactics and procedures for the destruction or removal of water pollutants are being studied [7-10].

Synthetic dyes and pigments are the most prevalent of the most dangerous organic pollutants. Organic compounds such as these, which are mostly produced by the discharge of food colorants, textiles, paper industries, printing, and other industries, can cause serious environmental problems. An example of these dyes, acid blue 342 which is a textile dye mainly used for wool, polyamide, silk dyeing and printing. It is an extremely hazardous, and excessive exposure to it causes a variety of health issues, including eye and skin irritations. [11].

Due to the limitation of water resources, one of the most pressing needs is the development of effective wastewater treatment techniques. Adsorption is thought to be environmentally friendly, highly effective, cost-efficient, and suited for practical applications [12]. Numerous materials, such as activated carbons (AC) [13], chitosan [14, 15], and mesoporous SiO_2 [16, 17], have been widely applied for the removal of organic dyes. The utility of adsorption phenomena could be expanded by using nanomaterials. Many researchers have been interested in wastewater as a result of recent advances in nanotechnology. Nanomaterial systems have numerous advantages, including the ability to be reused, ease of preparation, and great efficiency [18].

Various types of nanomaterials have recently been reported by various researchers. Nanoscale metal oxide, metal-based nanoparticles, polymer nanoparticles, zeolites, carbon-based nanomaterials, biopolymers, and metal-based nanoparticles have all been employed [19-21]. Amongst them is, metal oxide nanoparticles such as titanium dioxide (TiO_2), cerium oxide (CeO_2), zinc oxide (ZnO) and iron oxide (Fe_2O_3/Fe_3O_4), exhibiting a great adsorbent capacity for water purification [19]. Magnetic nanoparticles (MNPs) are a new branch of nanotechnology which are characterizes by a large specific surface area and short diffusion paths. Nanoparticles could be modified by functional groups on the surface [22-24]. Additionally, using an external magnetic field facilitates the separation of magnetic nanoparticles after treatment process [25-27].

Numerous types of MNPs have been fabricated and utilized for the purposes of water treatment [28-30], with chemical properties, varying sizes, and surface morphologies. Furthermore, the magnetic properties of these nanomaterials improve their ability to be removed from polluted media and also enhance their ability to be regenerated and reused [31, 32]. These MNPs act through three main steps, (i) pollutant migration to the adsorbent surface, (ii) binding to the surface of the adsorbent, and (iii) moving with the adsorbent.

As a result, the purpose of this research is to investigate the adsorption capacity of a textile dye Acid Blue 342 onto MNPs of Fe_2O_3/Fe_3O_4 nanocomposite. The optimization of the process is discussed based on the effects of different factors like contact time, dye concentration, value of pH and adsorbent dose on the adsorption capacity.

2. Experimental

Materials and Reagents

All materials and reagents in the current study were used as received without further purification since they were of analytical grade. Ferrous sulfate heptahydrate [$FeSO_4.7H_2O$, M.Wt (278.01 g/mole)] (Merk). Hexahydrated ferric chloride [$FeCl_3.6H_2O$, M.Wt (270.3 g/mole)], sodium hydroxide [NaOH, M.Wt (40 g/mole and Acid Blue 324 dye (AB 342) (Elnasr for chemicals, Egypt), Fig. (1).

Preparation of Fe_2O_3/Fe_3O_4 MNPs

Fe_2O_3/Fe_3O_4 nanocomposite was fabricated by using the coprecipitation method where, 8.4 g $FeSO_4.7H_2O$ was mixed and dissolved with 12.2 g $FeCl_3.6H_2O$ in 200 mL distilled water and furthermore the solution was stirred for 4 h [33]. At the same time, 50.0 mL of 6.5 M-NaOH was progressively added to that mixture, forming a black nanosized precipitate that was then washed numerous times with distilled water. After that, an external magnetic field was used to collect the precipitate in its pure state, which was then dried in a 70 °C oven.

3. Results and discussion

Characterization of MNPs

Zero of point charge (ZPC) of the nanocomposite

The Point of Zero Charge is the pH at which a solid surface has a net neutral charge (PZC). PZCs are one of the most important characteristics of an adsorbing solid or one with a pH-dependent surface charge, and they are closely linked to adsorbent qualities and adsorbing system applications [34]. The pH_{pzc} value was determined through the pH drift method [35]. The net surface charge of the adsorbent is positive at pH lower than pH_{pzc}, resulting in electrostatic repulsion with cationic species and perhaps inhibiting their adsorption from aqueous solutions. Due to the acidic dissociation of H^+ ions at pH levels greater than pHpzc, the surface charge of adsorbents has a net negative charge, favouring the absorption of positively charged species and repelling negatively charged sorbing species. The shift in pH of the aqueous dispersion (practical pH) is plotted against the initial pH (theoretical pH) values, the pH_{pzc} value is defined as the point where the $pH_{initial}–pH_{final}$ curve and the $pH_{initial}–pH_{final}$ line intersect. The pH_{pzc} value of the Fe_2O_3/Fe_3O_4 adsorbent was found to be around 6.45, consequently, it is preferred to remove anionic dye at pH < 6.45 to ensure that the net surface of the nanocomposite being positive, resulting in its affinity to attract anions **(Fig. 2)**. At pH above 6.45, the solid surface will be negatively charged, resulting in the repulsion of anions [36].

XRD study of Fe_2O_3/Fe_3O_4 nanoparticles

Powder X-ray diffraction (XRD) patterns obtained by an 18 kW diffractometer (Bruker; model D8 Advance) with monochromated Cu-K radiation (=1.54178 °A) were used to analyse the phase purity and structure of the as-synthesised Fe_2O_3/Fe_3O_4 nanocomposite. Maghemite/magnetite crystalline peaks were observed **(Fig. 3)** at 11.03°, 12.56°, 14.87°,18.31°, 23.70°, 29.96°, 30.27°, 33.90°, 35.30°, 43.25°, 53.54°, 57.16° and 62.72° assigned to the (101), (102), (103), (113), (106), (220), (206), (109), (311), (400), (442), (511) and (440) planes, respectively. All the main peaks can be indexed as both tetragonal maghemite (γ - Fe_2O_3) and cubic (Fe_3O_4) (space group: Fd-3 m) which are consistent with the standard pattern for JCPDS card No. (00-015-0615) and JCPDS card No. (00-002-1035), respectively. There were no typical peaks of additional impurity phases found, indicating that the resultant product was of high purity. Using the Scherrer formula, the crystallite size was calculated to be around 22.38 nm.

FT-IR study of Fe_2O_3/Fe_3O_4 nanoparticles

The FT-IR spectra of magnetic Fe_2O_3/Fe_3O_4 nanocomposites is presented in **Fig. 4.** The spectrum shows absorption bands at 1642 cm^{-1} and 3120 cm^{-1} which are assigned to O-H stretching mode. As shown in Fig. 4, the absorption band at 572.6 cm^{-1} is related to the stretching vibrations of Fe-O bonds of Fe_2O_3 and Fe_3O_4 nanoparticles [37].

Morphology study of Fe_2O_3/Fe_3O_4 nanoparticles

FE-SEM and HR-TEM images of Fe_2O_3/Fe_3O_4 nanoparticles

Morphologies of the as-prepared Fe_2O_3/Fe_3O_4 were investigated by using field emission scanning electron microscopy (FE-SEM) **(Fig. 5, a)** and High-resolution transmission electron microscopy (HR-TEM) **(Fig. 5, b)**. SEM is a type of electron microscope that scans a sample with a focused stream of electrons to predict images of it. When electrons contact with atoms in a sample, they produce a variety of signals that may be detected and carry information about the surface topography and composition of the sample**. (Fig. 5, a)**, presents secondary imaging analysis that was used for observation Fe_2O_3/Fe_3O_4 nanoparticles. The results of SEM analysis show rough surfaces and many visible fluffy mesoporous with a wide [38]. As shown in **(Fig. 5, b)**, the composite is composed of dispersed tetragonal and cubic particles which confirm the formation of both tetragonal maghemite (γ - Fe_2O_3) and cubic (Fe_3O_4) with an average diameter of 20-30 nm which is compatible with the crystalline size calculated from the XRD studies.

Adsorption experiments

Adsorption is a cost-effective and efficient method for treating wastewater containing chemically stable contaminants such heavy metals. The adsorption properties of the produced adsorbent were examined using (A B) dye as a hazardous contaminant. One of the parameters used to determine which sample is best for harmful dye removal procedure is its adsorption ability. The FT-IR spectra can be used as an evidence for the adsorption process of dyes[39, 40]. **Fig. 6 (a, b)**, depicts the FT-IR spectra of the prepared adsorbents before and after adsorption of (AB) dye. From **Fig. 6 (a, b)**, it is observed that the spectrum of (AB) dye-loaded for the adsorbent differs from that adsorbent before the adsorption, this is probably due to the adsorbed (AB) dye-loaded onto the adsorbent.

Many factors affect (AB) dye outflow from water were investigated, including pH, nanoparticle dose level, temperature, contact time, and heavy metal starting concentration. The adsorption tests have been carried out in batch mode, with (25-100 mg) of adsorbent charged into 25 mL of dye aqueous solution with a 50 mg L^{-1} starting concentration. The sorbent was collected on the inner wall of the glass container by applying a magnet after stirring for a specified amount of time (10-100

minutes). A UV–Vis spectrophotometer (Jasco-670, UV-visible spectrophotometer) was used to quantify the dye concentration in the remaining liquid phase. The removal efficiency (R) was calculated by the following equations:

$$R = \frac{C_0 - C_t}{C_0} \times 100 \quad (1)$$

The uptake of dyes (q_t, mg/g) at certain time (t, min) was evaluated by the following equation:

$$q_t = \frac{(C_0 - C_t)V}{W} \quad (2)$$

where C_0 (mg/L) was the initial mass concentration of dyes, C_t (mg/L) was the dyes concentration at time t, V (L) was the solution volume, and W (g) was the dosage of the sorbent.

Effect of pH

The pH of the working solution is a crucial factor in the solid extraction process because it affects the form of adsorbate and its surface charge. The effect of pH was investigated over the pH range 3.6–10.0. As shown in **Fig. 7**, AB removal reached a maximum value at a pH of 6.3. At pH 3.6, the solution turned to brown as a result of dissolution of iron oxides forming iron ions [41, 42]. The increase in electrostatic repulsion between the dye and the negative charges produced on the surface of nanoparticles caused a steady drop in the percentage of AB dyes adsorbed as the pH increased [43].

Effect of contact time and dye concentration

The effect of contact time on the removal efficiency of AB by Fe_2O_3/Fe_3O_4 MNPs is investigated at different contact time for varying dye concentrations (25, 50, 75, and 100 mg/L). As shown in **Fig. (8)**, It was observed that AB concentration decreases with increasing contact time and after 60 min, dye concentration decreases. With more increase in contact time from 60 to 100 min, the removal efficiency of MNPs increases very slightly. From the obtained result, it was found that the percentage removal of AB is inversely related to dye concentration. This shows that the adsorption process completely depends upon the area of active sites on the solid adsorbent which decreases as the initial concentration increases.

This assumes that the number of active binding sites is adequate to absorb a large number of AB molecules at lower dye concentrations, increasing the removal percent. However, at high AB concentrations, the available sorption sites become fewer, and the MNPs' sorption capacity remains constant, leaving more AB molecules in the solution. On the other hand, the loading capacity of the adsorbent (mg/g) could be evaluated depending on the concentration of the dye and adsorbent dose. The relation between loading capacity and initial dye concentration is presented in **Fig. (9)**. As shown in the figure, the increase of initial dye concentration results in a corresponding dye removal capacity. At the lowest concentration of AB, the removal capacity is 10.62 mg/g, while at 100 mg/L of dye the removal capacity is 39.45 mg/g.

Effect of adsorbent dose

The effect of nanoparticles dose on the AB removal efficiency for is shown in **Fig. 10**. The increase in the decolorization percentage is a function of the amount of adsorbent, due to the increase of the available adsorption sites. This result is in agreement with several other works [44, 45]. In most works dealing adsorption phenomenon, the dose of adsorbents affects the adsorption yield considerably. The removal percent was increased from 75.7 % to 89.3 % as the adsorbent dose increased from 1.0 to 2.5 g/L. At the same time, the removal efficiency (q_e) was decreased from 37.5 to 17.8 mg/g **(Fig. 11).**

Adsorption isotherms

When the dye removal process achieved equilibrium, different isotherm models were studied to see how AB dye molecules distributed between the aqueous adsorbate and solid adsorbent phases. The Langmuir, Freundlich, and Temkin results are essential because they provide information about the homogeneity/heterogeneity of the synthesised adsorbent as well as the design of various adsorption systems. The results are evaluated and the applicability of the models are generalized by comparing the correlation coefficient (R^2) of their linear fit.

Langmuir isotherm

The Langmuir isotherm [46], which suggests that elimination occurs at specified homogenous sites on the manufactured adsorbent, is extensively utilised in monolayer removal procedures. Equation (1) of the Langmuir model can be written as [46]:

$$\frac{C_e}{q_e} = \frac{1}{bq_{max}} + \frac{C_e}{q_{max}} \quad (3)$$

Where q_{max} (mg/g) represents the maximum adsorption capacity of an adsorbent, C_e is the equilibrium concentration of adsorbate (mg/L), q_e is the amount of dye adsorbed per gram of the adsorbent at equilibrium (mg/g), and b is the adsorption coefficient (L/mg). The linearized form of the Langmuir isotherm, assuming monolayer adsorption on a homogeneous adsorbent surface, is illustrated in **Fig. 12 (a)** for the removal of AB dye. **Table 1** contains Langmuir constants and coefficients. The essential parameters of Langmuir isotherm can be represented in term of dimensionless constant separation factor R_L that is given by Eq. (4):

$$R_L = \frac{1}{1 + bC_0} \quad (4)$$

Where C_0 (mg/L) is the initial concentration of adsorbate. The values of R_L are found to lie between 0.0056 and 0.0293 indicating that the dye removal is favorable ($0 < R_L < 1$) at the operating conditions.

Freundlich isotherm:

The Freundlich isotherm [47] describes the multilayers adsorption in heterogeneous systems. Freundlich model equation (5) may be represented by:

$$\ln q_e = \ln k_F + \frac{1}{n} \ln C_e \quad (5)$$

Where k_F and n are constants and q_e is the amount of dye adsorbed per gram of adsorbent at equilibrium (mg/g). This model is widely used for reversible

multilayer adsorption in heterogeneous systems with regular energy distribution. Freundlich plot, for the adsorptive removal of AB dye on the synthesized nano-adsorbent, is shown in **Fig. 12(b).** Further, Table 1 contains Freundlich constants and coefficients. The Constant n = 1.283 showing that the removal of AB dye was favorable.

Temkin isotherm [48]:

The linearized equation (4) for this model is given as:

$$q_e = B\ln A + B\ln C_e \quad (6)$$

where B (J/mol) and A (L/g) are constants that could be evaluated from the graph of q_e versus ln C_e. The constant B ($B = RT/b_T$) is a function of adsorption heat and A is the Temkin isotherm equilibrium binding constant which corresponds to the maximum binding energy. b_T is a the Temkin isotherm constant. Temkin isotherm plot, for the adsorptive removal of AB dye on the synthesized nano-adsorbent, is shown in **Fig. 12(c).** Further, **Table 1** contains Temkin isotherm constants and coefficients showing that the removal of AB dye was favorable. The viability of the adsorption models for the interpretation of the sorption process was investigated by computing the R^2 values of the three isotherms. As shown in Table (1), value obtained from the linear form of Langmuir equation is poorly compared with the experimental values. Based on the values if R^2, both Freundlich and Temkin models could be applied for the adsorption of AB dye on MNPs.

Kinetic Parameters

The study of adsorption kinetics is crucial for predicting the rate at which a pollutant can be removed from aqueous solutions and for understanding the mechanism of sorption events. The adsorption kinetic tests were done in batch mode with 100 mL of 75 mg L^{-1} AB dye solution at 35 ^{o}C. Pseudo-first-order and pseudo-second-order models were used to examine the mechanism of dye sorption onto Fe_2O_3/Fe_3O_4 MNPs. Pseudo-first-order rate equation is as follows: [49]

$$\ln(q_e - q_t) = \ln q_e - k_1 t \quad (7)$$

where q_e and qt are the amounts of dye adsorbed (mg/g) at equilibrium and at time t (min) respectively and k_1 (min) is the pseudo-first-order rate constant. Values of k_1 were calculated from the plot of ln (q_e-q_t) versus t **(Fig. 13)**.

The rate equation for Ho's pseudo-second-order model [50] is given by:

$$t/q_t = 1/k_2 q_e^2 + t/q_e \quad (8)$$

where k_2 (g/mg min) is the pseudo-second-order rate constant and its value was obtained from the plot of t/q_t vs. t **(Fig. 14)**.

The q values experimental from pseudo first-ordered kinetic model were too small compared the calculated Value for AB dye. The experimental value qe from the pseudo-second-order kinetic model, on the other hand, was rather close to the calculated value.These findings suggested that the pseudo second-order adsorption mechanism is dominant, and that the chemisorption process appears to influence the overall rate of the AB dye adsorption process. The kinetic results were also analyzed by intra-particle diffusion model to gain further insight into the adsorption behavior of the dye on Fe_2O_3/Fe_3O_4 nanoparticles. The obtained k_1 and k_2 values for Fe_2O_3/Fe_3O_4 nanocomposite plus other parameters obtained from the linear form of pseudo-first-order and pseudo-second-order are listed in **Table 2**. The rate determining step in liquid/solid adsorption systems can be determined using this approach. A boundary layer or intra-particle diffusion of solute to the solid surface from the bulk of the solution could be the rate limiting step. The prospect of the intra-particle diffusion model is explored by using the modified Weber and Morris [51] equation:

$$q_t = k_{dif} t^{0.5} + C \quad (9)$$

where q_t is adsorption capacity at any time t and k_{dif} is the intraparticle diffusion rate constant (mg/g $min^{½}$) and C is the film thickness. The values of k_{dif} and C could be calculated from the slope and intercept of plots of qt versus $t^{0.5}$ (Fig. 15). If intra-particle diffusion is the rate limiting step, the plot of qt vs. square root of time should be a straight line passing through the origin with C = 0. The resultant figure **(Fig. 15)** does not pass the origin in this example, indicating that the overall adsorption process may be mediated by multiple mechanisms including film diffusion, chemical reaction, and intra-particle diffusion [52, 53].

Table (1) Adsorption isotherms parameters of AB on MNPs.

Langmuir				Freundlich			Temkin		
q_m	b	R_L (L/mg)	R^2	1/n	K_F ((mg/g)(L/mg)$^{1/n}$	R^2	B	A	R^2
100	0.0326	0.234	0.9610	0.779	3.9174	0.9876	16.96	0.4786	0.9889

Table (2) Adsorption isotherms parameters of AB on MNPs.

Pseudo-first-ordered model				Pseudo-second-ordered model		
$q_{e\ (cal)}$ (mg/g)	$q_{e\ (exp)}$ (mg/g)	K_1	R^2	$q_{e\ (exp)}$ (mg/g)	K_2	R^2
39.45	27.504	0.0516	0.9018	43.454	0.0016	0.9992

4. Conclusion

A facile nanocomposite of Fe2O3/Fe3O4 MNPs was synthesized via coprecipitation method. The structure of the as-prepared adsorbents was studied using FT-IR, SEM, TEM, and XRD techniques, and a putative mechanism for nanocomposite production was proposed. After that, the nanocomposite was used as an excellent adsorbent to remove Acid blue colour 342 dye (AB). The experimental data fit well with the pseudo-second-order and Langmuir isotherm models, according to the kinetics and isotherm modelling studies. The maximum capacity of the adsorbent was found to be 45.45 mg/g for AB dye. All obtained results depict that the fabricated Fe2O3/Fe3O4 MNPs nanocomposite can be used as an effective, easily separable, and reusable adsorbent for the removal of toxic Acid blue dye 342 dye from aqueous solution

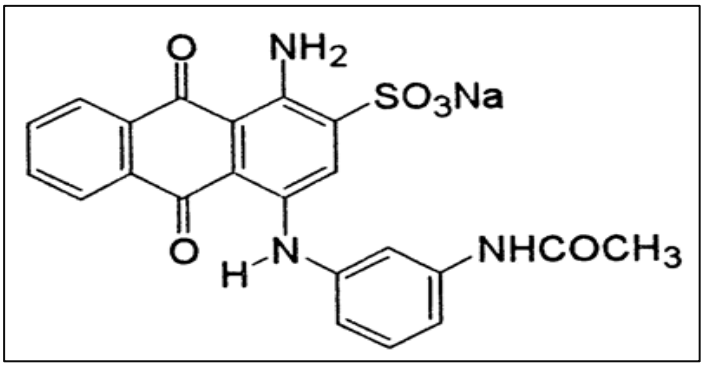

Fig. (1) Chemical structure of Acid Blue 324

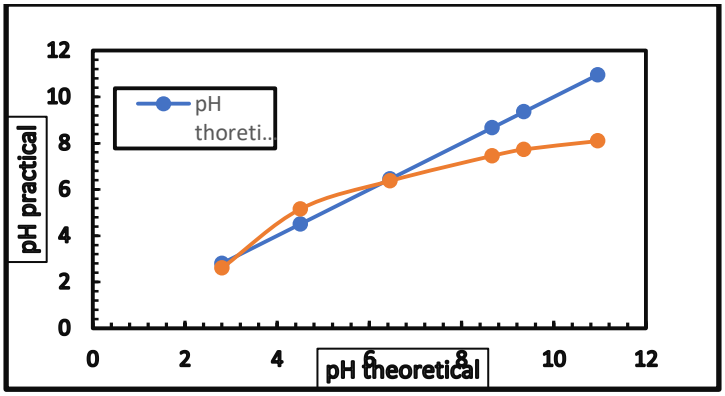

Fig. (2) Determination of ZPC of Fe_3O_4 /Fe_2O_3 MNPs

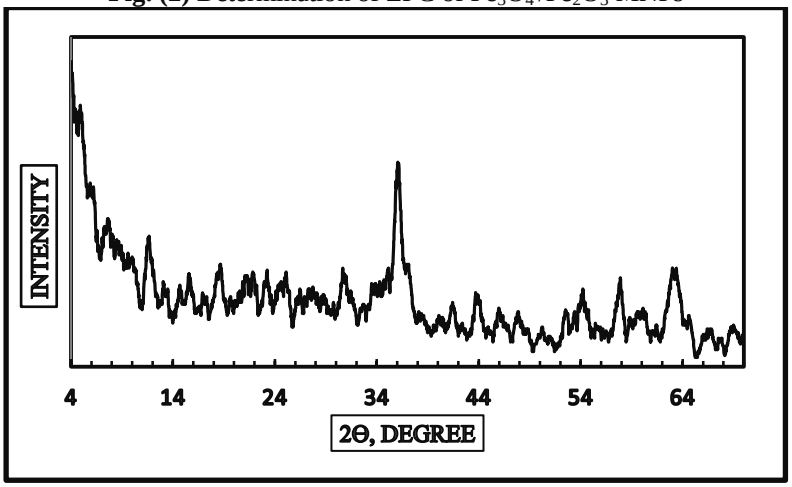

Fig. (3) XRD of Fe_3O_4 /Fe_2O_3 MNPs

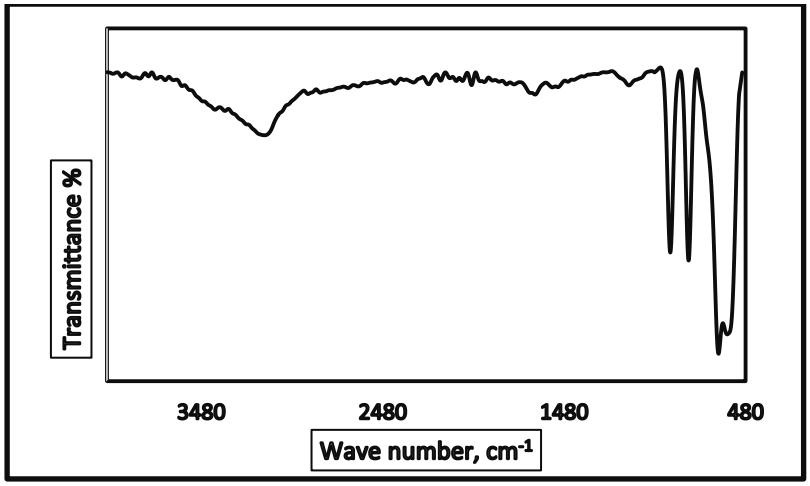

Fig. (4) FT-IR spectra of Fe_3O_4 /Fe_2O_3 MNPs

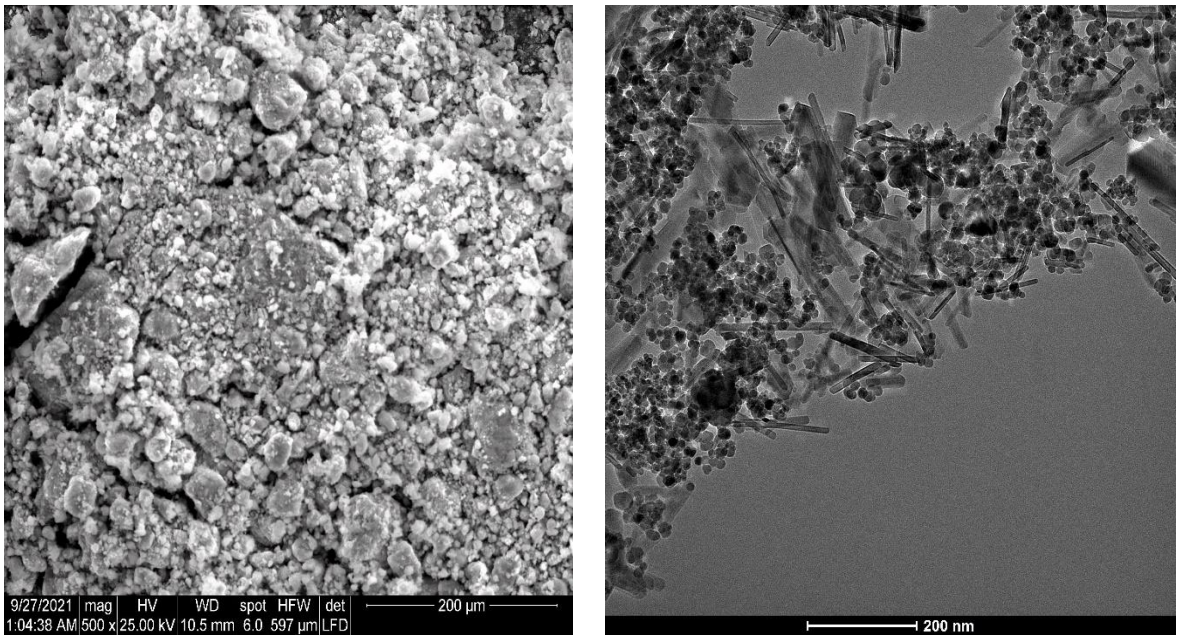

(a) **(b)**

Fig. (5) SEM image (a) and TEM image (b) of Fe_3O_4 /Fe_2O_3 MNPs

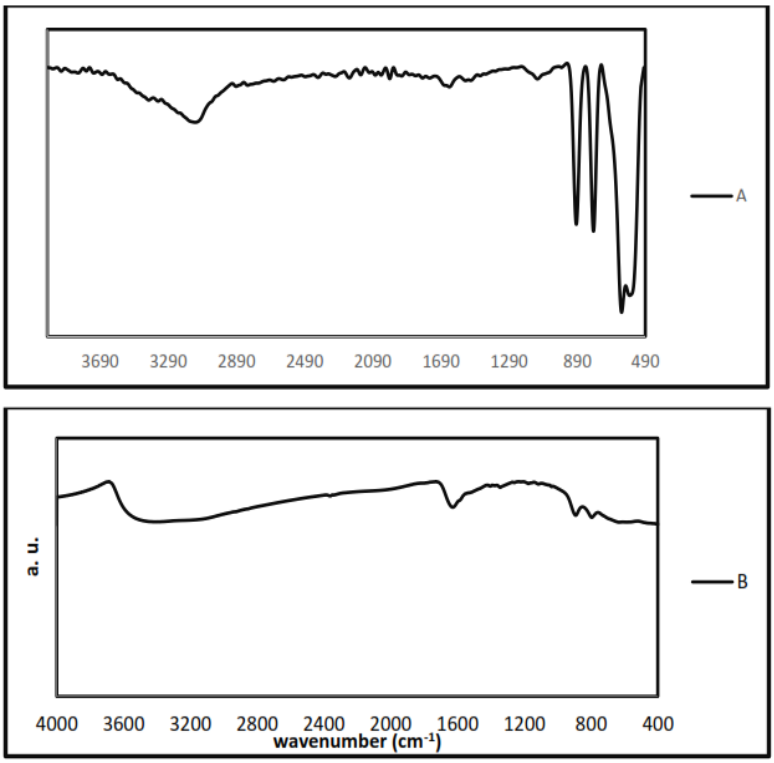

Fig. (6) The FT-IR spectra of the Fe_3O_4 /Fe_2O_3 before (A) and after (B) the adsorption of (AB).

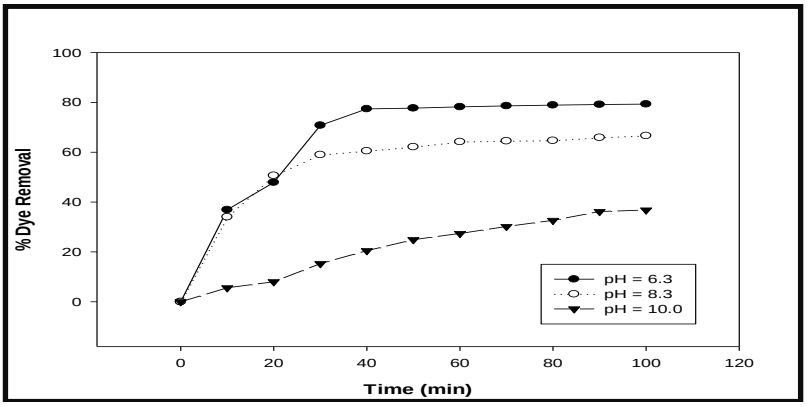

Fig. (7) Effect of pH on removal of AB by Fe_3O_4 /Fe_2O_3 MNPs ([AB] = 50 mg/L, Dose = 1 g/L, rpm = 700)

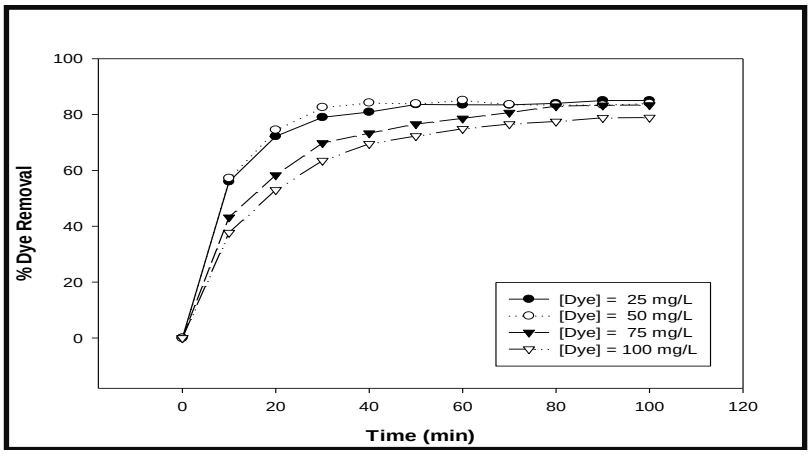

Fig. (8) Effect of contact time on AB removal percent by Fe_2O_3/Fe_3O_4 MNPs for different dye concentrations [Fe_2O_3/Fe_3O_4 = 1 g/L, pH = 6.3].

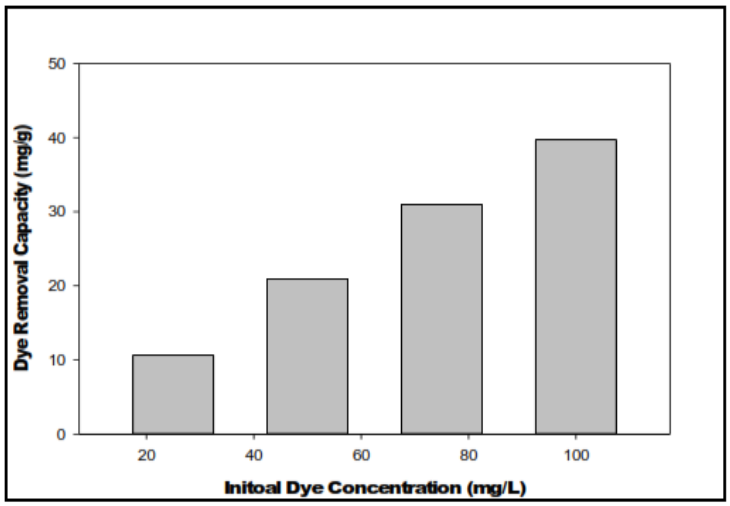

Fig. (9) Effect of different dye concentrations on AB removal capacity by Fe_2O_3/Fe_3O_4 MNPs for [dose = 1.0 g/L, pH = 6.3].

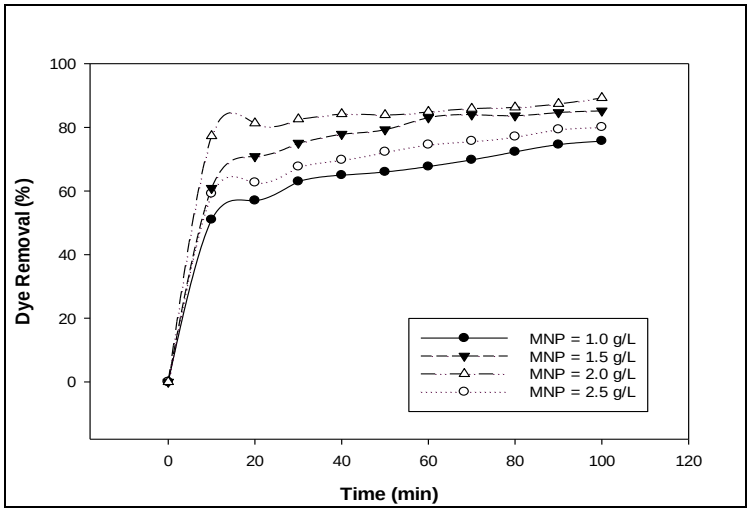

Fig. (10) Effect of contact time on AB removal by different doses of Fe_2O_3/Fe_3O_4 MNPs [AB conc. = 0.1 g/L, pH = 6.3].

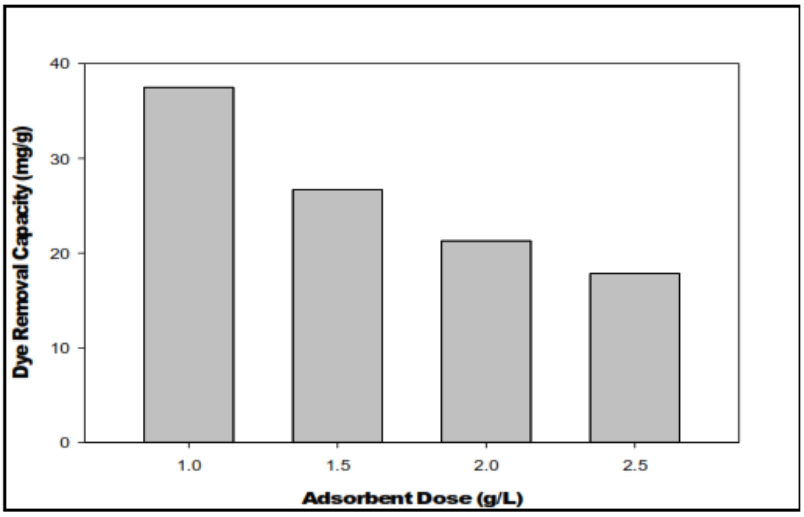

Fig. (11) Effect of MNPs on AB removal capacity by Fe_3O_4 [AB] = 0.1 g/L, pH = 6.3].

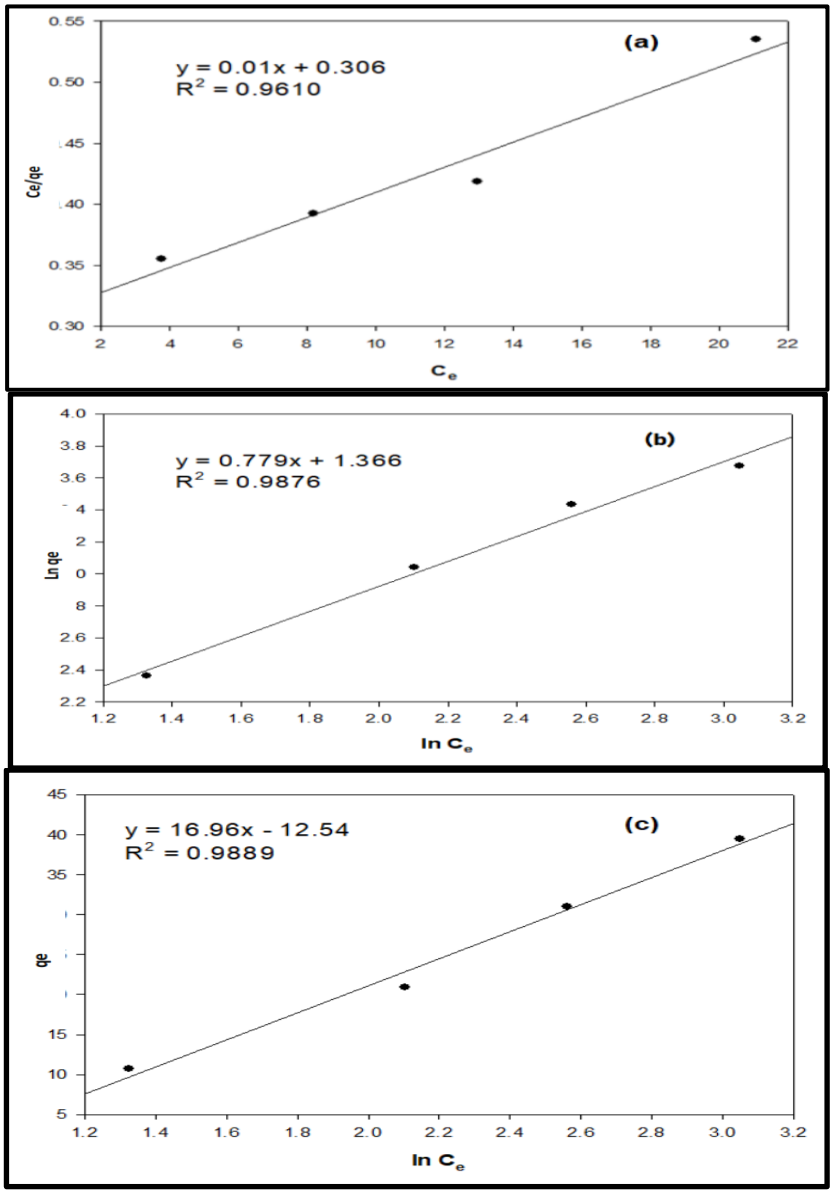

Fig. (12) (a-c) Linear plots of Langmuir (a), Freundlich (b) and Temkin isotherm (c) equations for adsorption of AB on Fe_2O_3/Fe_3O_4 MNPs.

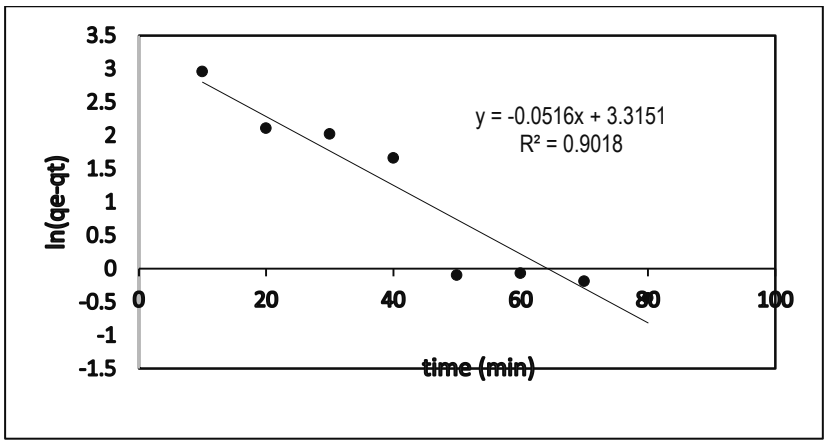

Fig. (13) Pseudo-first-order plots for adsorption of AB dye (100 mg/L) on Fe_2O_3/Fe_3O_4 MNPs.

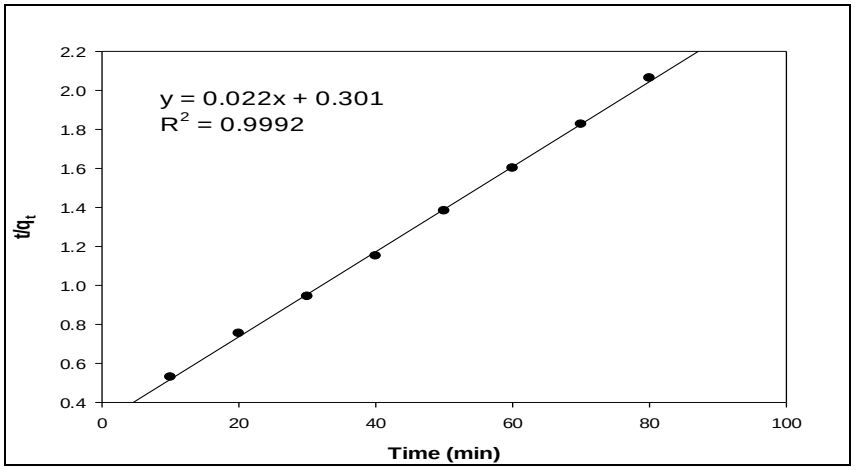

Fig. (14) Pseudo-second-order plots for adsorption of AB dye (100 mg/L) on Fe_2O_3/Fe_3O_4 MNPs.

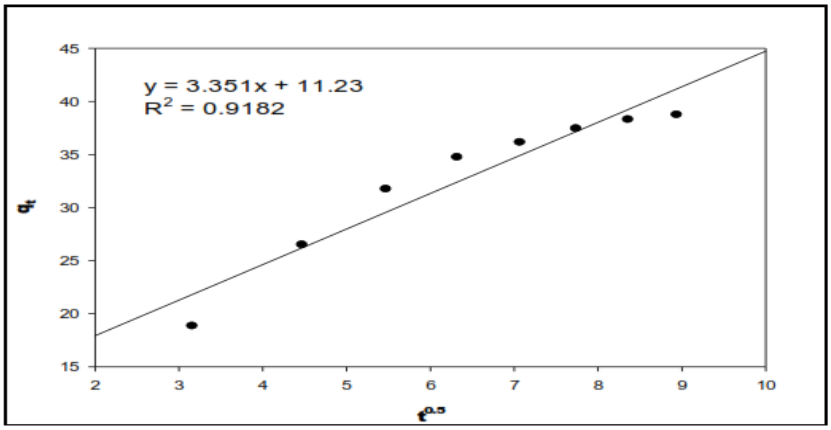

Fig. (15) Intra-particle diffusion model for the adsorption of AB dye onto Fe_2O_3/Fe_3O_4 MNPs.

References

[1] Liu, X., et al., A valuable biochar from poplar catkins with high adsorption capacity for both organic pollutants and inorganic heavy metal ions. 2017. **7**(1): p. 1-12.

[2] Mahlambi, M.M., et al., β-Cyclodextrin-ionic liquid polyurethanes for the removal of organic pollutants and heavy metals from water: synthesis and characterization. 2010. **17**(4): p. 589-600.

[3] Wright, I.A. and S.J.H. Burgin, Effects of organic and heavy metal pollution on chironomids within a pristine upland catchment. 2009. **635**(1): p. 15-25.

[4] Shukla, S., et al., Synthesis and characterization of magnetic nanoparticles, and their applications in wastewater treatment: A review. 2021: p. 101924.

[5] Chen, C.-Y., et al., Non-Conventional Water Reuse in Agriculture: A Circular Water Economy. 2021: p. 117193.

[6] Akpor, O. and B.J.A.J.o.B. Muchie, Environmental and public health implications of wastewater quality. 2011. **10**(13): p. 2379-2387.

[7] Aqeel, K., et al. Electrochemical removal of brilliant green dye from wastewater. in IOP Conference Series: Materials Science and Engineering. 2020. IOP Publishing.

[8] Piaskowski, K., R. Świderska-Dąbrowska, and P.K.J.J.o.A.I. Zarzycki, Dye removal from water and wastewater using various physical, chemical, and biological processes. 2018. **101**(5): p. 1371-1384.

[9] Katheresan, V., J. Kansedo, and S.Y.J.J.o.e.c.e. Lau, Efficiency of various recent wastewater dye removal methods: A review. 2018. **6**(4): p. 4676-4697.

[10] Hesham H. El-Feky1*, R.N.N., Alaa S. Amin1*, Mostafa Y. Nassar1* %J asian journal of chemical sciences, Removal of Malachite Green Dye from Aqueous Solutions by an Efficient Nanosized NiO Fabricated by a Facile Sol-Gel Autocombustion. 2021. **10**(2): p. 41-51.

[11] Özer, A., G. Akkaya, and M.J.J.o.h.m. Turabik, Biosorption of acid blue 290 (AB 290) and acid blue 324 (AB 324) dyes on Spirogyra rhizopus. 2006. **135**(1-3): p. 355-364.

[12] Liu, L., et al., Adsorption removal of dyes from single and binary solutions using a cellulose-based bioadsorbent. 2015. **3**(3): p. 432-442.

[13] Djilani, C., et al., Adsorption of dyes on activated carbon prepared from apricot stones and commercial activated carbon. 2015. **53**: p. 112-121.

[14] Dotto, G.L. and L.A.d.A.J.C.P. Pinto, Adsorption of food dyes onto chitosan: Optimization process and kinetic. 2011. **84**(1): p. 231-238.
[15] Wong, Y., et al., Adsorption of acid dyes on chitosan—equilibrium isotherm analyses. 2004. **39**(6): p. 695-704.
[16] Thu, H.T., L.T. Dat, and V.A.J.V.J.o.C. Tuan, Synthesis of mesoporous SiO2 from rice husk for removal of organic dyes in aqueous solution. 2019. **57**(2): p. 175-181.
[17] Cui, R., et al., Two-dimensional porous SiO2 nanostructures derived from renewable petal cells with enhanced adsorption efficiency for removal of hazardous dye. 2017. **5**(4): p. 3478-3487.
[18] Borji, H., et al., How effective are nanomaterials for the removal of heavy metals from water and wastewater? 2020. **231**(7): p. 1-35.
[19] Ali, I., et al., Water purification using magnetic nanomaterials: an overview. 2019: p. 161-179.
[20] Shan, S., et al. A mini-review of carbonaceous nanomaterials for removal of contaminants from wastewater. in IOP Conference Series: Earth and Environmental Science. 2017. IOP Publishing.
[21] Naseem, T., T.J.E.C. Durrani, and Ecotoxicology, The role of some important metal oxide nanoparticles for wastewater and antibacterial applications: A review. 2021.
[22] Faraji, M., Y. Yamini, and M.J.J.o.t.I.C.S. Rezaee, Magnetic nanoparticles: synthesis, stabilization, functionalization, characterization, and applications. 2010. **7**(1): p. 1-37.
[23] Ge, F., et al., Efficient removal of cationic dyes from aqueous solution by polymer-modified magnetic nanoparticles. 2012. **198**: p. 11-17.
[24] Yang, H., et al., Rapid removal of anionic dye from water by poly (ionic liquid)-modified magnetic nanoparticles. 2019. **284**: p. 383-392.
[25] Wang, X., et al., Synthesis of chitosan/poly (ethylene glycol)-modified magnetic nanoparticles for antibiotic delivery and their enhanced anti-biofilm activity in the presence of magnetic field. 2018. **53**(9): p. 6433-6449.
[26] Fatima, H. and K.-S.J.K.J.o.C.E. Kim, Magnetic nanoparticles for bioseparation. 2017. **34**(3): p. 589-599.
[27] Suleiman, J.S., et al., Separation/preconcentration of trace amounts of Cr, Cu and Pb in environmental samples by magnetic solid-phase extraction with Bismuthiol-II-immobilized magnetic nanoparticles and their determination by ICP-OES. 2009. **77**(5): p. 1579-1583.
[28] Mohammed, L., et al., Magnetic nanoparticles for environmental and biomedical applications: A review. 2017. **30**: p. 1-14.
[29] Rios, A., M. Zougagh, and M.J.A.M. Bouri, Magnetic (nano) materials as an useful tool for sample preparation in analytical methods. A review. 2013. **5**(18): p. 4558-4573.
[30] Joo, S.H. and D.J.J.o.H.M. Zhao, Environmental dynamics of metal oxide nanoparticles in heterogeneous systems: A review. 2017. **322**: p. 29-47.
[31] Kefeni, K.K., et al., Application of spinel ferrite nanoparticles in water and wastewater treatment: a review. 2017. **188**: p. 399-422.
[32] Rivas, B.L., B.F. Urbano, and J.J.F.i.c. Sánchez, Water-soluble and insoluble polymers, nanoparticles, nanocomposites and hybrids with ability to remove hazardous inorganic pollutants in water. 2018. **6**: p. 320.
[33] Mahmoud, M.E., M.S. Abdelwahab, and E.M.J.C.E.J. Fathallah, Design of novel nano-sorbents based on nano-magnetic iron oxide–bound-nano-silicon oxide–immobilized-triethylenetetramine for implementation in water treatment of heavy metals. 2013. **223**: p. 318-327.
[34] Yu, M., et al., Model prediction of the point of zero net charge of layered double hydroxides and clay minerals. 2021. **611**: p. 125860.
[35] Baena-Garcıa, M., et al. Early drift detection method. in Fourth international workshop on knowledge discovery from data streams. 2006.
[36] Wang, Z., et al., Dually organic modified bentonite with enhanced adsorption and desorption of tetracycline and ciprofloxacine. 2021: p. 119059.
37] Molodtsova, T., et al., One-step synthesis of γ-Fe2O3/Fe3O4 nanocomposite for sensitive electrochemical detection of hydrogen peroxide. 2021. **370**: p. 137723.
38] Smith, K. and C.J.B.J.o.A.P. Oatley, The scanning electron microscope and its fields of application. 1955. **6**(11): p. 391.
[39] Li, S., Combustion synthesis of porous MgO and its adsorption properties. International Journal of Industrial Chemistry, 2019. **10**(1): p. 89-96.
[40] Nassar, M.Y., et al., MgO nanostructure via a sol-gel combustion synthesis method using different fuels: An efficient nano-adsorbent for the removal of some anionic textile dyes. Journal of Molecular Liquids, 2017. **225**: p. 730-740.
[41] Salmimies, R., P. Vehmaanperä, and A.J.H. Häkkinen, Acidic dissolution of magnetite in mixtures of oxalic and sulfuric acid. 2016. **163**: p. 91-98.
[42] Salmimies, R., et al., Acidic dissolution of magnetite: experimental study on the effects of acid concentration and temperature. 2011. **59**(2): p. 136-146.
[43] Saheed, I.O., W.-D. Oh, and F.B.M.J.I.J.o.B.M. Suah, Enhanced adsorption of acid Blue-25 dye onto chitosan/porous carbon composite modified in 1-allyl-3-methyl imidazolium bromide ionic liquid. 2021. **183**: p. 1026-1033.
[44] El Khomri, M., et al., Efficient adsorbent derived from Argania Spinosa for the adsorption of cationic dye: Kinetics, mechanism, isotherm and thermodynamic study. 2020. **20**: p. 100601.
[45] Shakoor, S. and A.J.J.o.t.T.I.o.C.E. Nasar, Removal of methylene blue dye from artificially

contaminated water using citrus limetta peel waste as a very low cost adsorbent. 2016. **66**: p. 154-163.
[46] Langmuir, I.J.J.o.t.A.c.s., The constitution and fundamental properties of solids and liquids. Part I. Solids. 1916. **38**(11): p. 2221-2295.
[47] Freundlich, H.J.J.P.c., Over the adsorption in solution. 1906. **57**(385471): p. 1100-1107.
[48] Temkin, M.I.J.Z.F.C., Adsorption equilibrium and the kinetics of processes on nonhomogeneous surfaces and in the interaction between adsorbed molecules. 1941. **15**: p. 296-332.
[49] Lagergren, S., Zur theorie der sogenannten adsorption geloster stoffe. 1898.
[50] Ho, Y.-S.J.J.o.h.m., Review of second-order models for adsorption systems. 2006. **136**(3): p. 681-689.
[51] Weber, W., JC Morris in: Proc. Int. Conf. Water Pollution Symposium, vol. 2. 1962, Pergamon, Oxford.
[52] Hou, S.X. Adsorption properties of pomelo peels against methylene blue in dye wastewater. in Advanced Materials Research. 2013. Trans Tech Publ.
[53] Dawood, S. and T.K.J.W.r. Sen, Removal of anionic dye Congo red from aqueous solution by raw pine and acid-treated pine cone powder as adsorbent: equilibrium, thermodynamic, kinetics, mechanism and process design. 2012. **46**(6): p. 1933-1946.